Available online at www.sciencedirect.com
SCIENCE DIRECT®
Journal of Solid State Chemistry 177 (2004) 2523–2529
JOURNAL OF SOLID STATE CHEMISTRY
http://elsevier.com/locate/jssc

Ternary silicides $M_2Cr_4Si_5$ (M = Ti, Zr, Hf): filled variants of the Ta_4SiTe_4 structure type

Shane J. Crerar and Arthur Mar*

Department of Chemistry, University of Alberta, Edmonton, Alberta, Canada T6G 2G2

Received 18 December 2003; received in revised form 23 March 2004; accepted 28 March 2004

Abstract

The isostructural ternary silicides $M_2Cr_4Si_5$ (M = Ti, Zr, Hf) were prepared by arc-melting of the elemental components. The single-crystal structure of $Zr_2Cr_4Si_5$ was determined by X-ray diffraction (Pearson symbol *oI*44, orthorhombic, space group *Ibam*, $Z = 4$, $a = 7.6354(12)$ Å, $b = 16.125(3)$ Å, $c = 5.0008(8)$ Å). $Zr_2Cr_4Si_5$ adopts the $Nb_2Cr_4Si_5$-type structure, an ordered variant of the V_6Si_5-type structure. It consists of square antiprisms that have Zr and Cr atoms at the corners and Si atoms at the centers; they share opposite faces to form one-dimensional chains $^1_\infty[Zr_{4/2}Cr_{4/2}Si]$ surrounded by additional Si atoms and extending along the c direction. In a new interpretation of the structure, additional Cr atoms occupy interstitial octahedral sites between these chains, clarifying the relation between this structure and that of Ta_4SiTe_4. The formation of short Si–Si bonds in $Zr_2Cr_4Si_5$ is contrasted with the absence of Te–Te bonds in Ta_4SiTe_4. The compounds $M_2Cr_4Si_5$ (M = Ti, Zr, Hf) exhibit metallic behavior and essentially temperature-independent paramagnetism. Bonding interactions were analyzed by band structure calculations, which confirm the importance of Si–Si bonding in these metal-rich compounds.

Keywords: Zirconium; Chromium; Silicide; Crystal structure; Band structure

1. Introduction

Several ternary transition-metal silicides $M_{6-x}M'_xSi_5$ (M, M' = Sc, Ti, Zr, Hf, V, Nb, Ta, Cr, Mn) [1–7] adopt an ordered version of the structure of V_6Si_5 (or Ti_6Ge_5) [8] called the $Nb_2Cr_4Si_5$-type [1]. Identified as the θ-phase in the Nb–Cr–Si system, $Nb_2Cr_4Si_5$ adopts a typical intermetallic structure containing densely packed layers of atoms [1]. Three possible sites are available to be occupied by the two types of transition metals. If M is the earlier and M' is the later transition metal, the most commonly encountered composition is $M_2M'_4Si_5$. A limited range of solid solution occurs in some systems, depending on the relative sizes of the metal atoms and the site occupation preferences. For example, $Nb_2Cr_4Si_5$ and $Nb_4Cr_2Si_5$ represent end members of a solid solution $Nb_{6-x}Cr_xSi_5$ ($2 \leqslant x \leqslant 4$) [5].

Recently, we demonstrated that quaternary antimonides such as $Nb_4Pd_{0.5}SiSb_2$ represent filled variants of the V_4SiSb_2-type structure, in which Pd atoms partially occupy *tetrahedral* sites between one-dimensional chains of face-sharing Si-centered square antiprisms $^1_\infty[Nb_{8/2}Si]$ encapsulated by Sb atoms [9]. We wondered whether the related Ta_4SiTe_4-type structure could serve as a host in which *octahedral* sites between similar one-dimensional chains $^1_\infty[Ta_{8/2}Si]$ encapsulated by Te atoms could be occupied by interstitial atoms [10,11].

The series $M_2Cr_4Si_5$ (M = Ti, Zr, Hf) has previously been reported [3,4], but no single-crystal diffraction work has been forthcoming to verify if an ordered structure is adopted. No reports of the physical properties of any of these silicides $M_{6-x}M'_xSi_5$ have appeared. We present here the synthesis of the ternary silicides $M_2Cr_4Si_5$ (M = Ti, Zr, Hf), the crystal structure of $Zr_2Cr_4Si_5$, and electrical and magnetic measurements on the entire series. We show that $Zr_2Cr_4Si_5$ represents the sought-after filled variant of the Ta_4SiTe_4-type structure in which Cr atoms occupy octahedral sites, and analyze

*Corresponding author. Fax: +780-492-8231.
E-mail address: arthur.mar@ualberta.ca (A. Mar).

0022-4596/$ - see front matter © 2004 Elsevier Inc. All rights reserved.
doi:10.1016/j.jssc.2004.03.040

the bonding in this structure through extended Hückel band structure calculations.

2. Experimental

2.1. Synthesis

The single crystal of $Zr_2Cr_4Si_5$ used for the structure determination was originally obtained as an adventitious product in the course of investigating the Zr–Cr–Sb system. Zr, Cr, and Sb were reacted in a 8:1:1 ratio in the presence of an Sn flux in an evacuated fused-silica tube at 1000°C for 1 week and 600°C for 24 h, resulting in black needle-shaped crystals. Energy-dispersive X-ray (EDX) analysis on a Hitachi S-2700 scanning electron microscope confirmed the presence of all three elements (and the absence of other elements) in these crystals, including that used for the X-ray data collection. Incorporation of silicon evidently occurred as a result of attack of the silica tube, as is sometimes observed. For example, recent investigations suggest that "β-$ZrSb_2$" prepared in a silica tube is really a ternary compound, $ZrSi_\delta Sb_{2-\delta}$ [12]. Subsequently, stoichiometric mixtures of the elemental powders (Ti, 99.98%; Zr, 99.7%; Hf, 99.6%; Cr, 99.95%; Si, 99.96%; all from Cerac except Hf from Alfa-Aesar) were pressed into pellets and reacted on a 0.25-g scale by arc-melting in a Centorr 5TA tri-arc furnace under argon (gettered by melting a titanium pellet). Microcrystals extracted from the arc-melted products were confirmed by EDX analysis to contain all three elements. Yields of $M_2Cr_4Si_5$ (M = Ti, Zr, Hf) were essentially quantitative, as ascertained by X-ray powder diffraction on an Enraf–Nonius FR552 Guinier camera. Cell parameters were refined with use of the program POLSQ [13] and are listed in Table 1. In particular, the cell parameters and the diffraction intensities calculated from the single-crystal structure of $Zr_2Cr_4Si_5$ are in good agreement with the powder data.

2.2. Structure determination

Intensity data were collected on a Bruker Platform/SMART 1000 CCD at 22°C using ω scans (0.2°). Crystal data are given in Table 2. Calculations were carried out with use of the SHELXTL (version 5.1) package [14]. Face-indexed numerical absorption corrections were applied. The centrosymmetric space group *Ibam* was chosen and initial atomic positions were found by direct methods. Refinements proceeded in a straightforward manner, and revealed no evidence for partial occupancy or disorder of sites. The final-difference electron density map is featureless. The atomic positions were standardized with the program STRUCTURE TIDY [15]; note that this standardization interchanges the labels of the Si1 and Si2 atoms compared to previous

Table 1
Cell parameters for $M_2Cr_4Si_5$ (M = Ti, Zr, Hf)

Compound	a (Å)	b (Å)	c (Å)	V (Å^3)
$Ti_2Cr_4Si_5$	7.496(8)	15.92(1)	4.878(4)	581.9(6)
$Zr_2Cr_4Si_5$	7.630(3)	16.137(8)	4.979(2)	613.1(3)
$Hf_2Cr_4Si_5$	7.608(3)	16.103(7)	4.967(2)	608.5(3)

Table 2
Crystallographic data for $Zr_2Cr_4Si_5$

Formula	$Zr_2Cr_4Si_5$
Formula mass (amu)	530.89
Space group	D_{2h}^{26}–*Ibam* (No. 72)
a (Å)[a]	7.6354(12)
b (Å)[a]	16.125(3)
c (Å)[a]	5.0008(8)
V (Å^3)	615.7(2)
Z	4
ρ_{calcd} (g cm^{-3})	5.727
Crystal dimensions (mm)	$0.12 \times 0.02 \times 0.01$
Radiation	Graphite monochromated Mo$K\alpha$, $\lambda = 0.71073$ Å
μ(Mo$K\alpha$) (cm^{-1})	109.21
Transmission factors	0.459–0.898
2θ limits	$5.06° \leqslant 2\theta(\text{Mo}K\alpha) \leqslant 52.58°$
Data collected	$-9 \leqslant h \leqslant 9$, $-20 \leqslant k \leqslant 20$, $-5 \leqslant l \leqslant 6$
No. of data collected	2187
No. of unique data, including $F_o^2 < 0$	358
No. of unique data, with $F_o^2 > 2\sigma(F_o^2)$	327
No. of variables	33
$R(F)$ for $F_o^2 > 2\sigma(F_o^2)$[b]	0.038
$R_w(F_o^2)$[c]	0.097
Goodness of fit	1.276
$(\Delta\rho)_{max}$, $(\Delta\rho)_{min}$ (e Å^{-3})	2.01, −0.99

[a] Obtained from a refinement constrained so that $\alpha = \beta = \gamma = 90°$.
[b] $R(F) = \sum||F_o| - |F_c||/\sum|F_o|$.
[c] $R_w(F_o^2) = \left[\sum[w(F_o^2 - F_c^2)^2]/\sum wF_o^4\right]^{1/2}$; $w^{-1} = [\sigma^2(F_o^2) + (0.0514p)^2 + 5.9458p]$ where $p = [\max(F_o^2, 0) + 2F_c^2]/3$.

Table 3
Atomic coordinates and equivalent isotropic displacement parameters for $Zr_2Cr_4Si_5$

Atom	Wyckoff position	x	y	z	U_{eq} (Å^2)[a]
Zr	8*j*	0.37874(12)	0.35863(5)	0	0.0033(3)
Cr1	8*j*	0.2529(2)	0.06119(9)	0	0.0040(4)
Cr2	8*g*	0	0.30889(9)	1/4	0.0043(4)
Si1	8*j*	0.0736(4)	0.43587(16)	0	0.0062(6)
Si2	8*j*	0.2070(4)	0.21121(16)	0	0.0047(6)
Si3	4*a*	0	0	1/4	0.0027(8)

[a] U_{eq} is defined as one-third of the trace of the orthogonalized U_{ij} tensor.

Table 4
Selected interatomic distances (Å) for $Zr_2Cr_4Si_5$

Zr–Si1	2.642(3)
Zr–Si2	2.715(3)
Zr–Si2	2.748(3)
Zr–Si3	2.760(1) (× 2)
Zr–Si2	2.819(1) (× 2)
Zr–Cr1	2.989(1) (× 2)
Zr–Cr2	3.117(2) (× 2)
Zr–Cr1	3.136(2)
Zr–Cr2	3.251(1) (× 2)
Zr–Cr1	3.418(2)
Zr–Zr	3.111(1) (× 2)
Cr1–Si1	2.416(3)
Cr1–Si2	2.444(3)
Cr1–Si1	2.449(3)
Cr1–Si3	2.503(1) (× 2)
Cr1–Si1	2.830(2) (× 2)
Cr1–Cr2	3.084(2) (× 2)
Cr1–Cr1	3.185(2) (× 2)
Cr1–Zr	2.989(1) (× 2)
Cr1–Zr	3.136(2)
Cr1–Zr	3.418(2)
Cr2–Si1	2.464(3) (× 2)
Cr2–Si2	2.558(3) (× 2)
Cr2–Si2	2.583(2) (× 2)
Cr2–Cr2	2.5004(4) (× 2)
Cr2–Cr1	3.084(2) (× 2)
Cr2–Zr	3.117(2) (× 2)
Cr2–Zr	3.251(1) (× 2)
Si1–Si1	2.354(5)
Si1–Si1	2.742(2) (× 2)
Si1–Cr1	2.416(3)
Si1–Cr1	2.449(3)
Si1–Cr2	2.464(3) (× 2)
Si1–Cr1	2.830(2) (× 2)
Si1–Zr	2.642(3)
Si2–Si2	2.872(3) (× 2)
Si2–Cr1	2.444(3)
Si2–Cr2	2.558(3) (× 2)
Si2–Cr2	2.583(2) (× 2)
Si2–Zr	2.715(3)
Si2–Zr	2.748(3)
Si2–Zr	2.819(1) (× 2)
Si3–Si3	2.5004(4) (× 2)
Si3–Cr1	2.503(1) (× 4)
Si3–Zr	2.760(1) (× 4)

structure determinations on V_6Si_5 [8], $Sc_2Cr_4Si_5$ [6], $Nb_2Cr_4Si_5$ [1], or $Nb_4Cr_2Si_5$ [5]. Final values of the positional and displacement parameters are given in Table 3. Interatomic distances are listed in Table 4. Further data, in the form of a CIF, have been sent to Fachinformationszentrum Karlsruhe, Abt. PROKA, 76344 Eggenstein–Leopoldshafen, Germany, as supplementary material No. CSD–413890 and can be obtained by contacting FIZ (quoting the article details and the corresponding CSD numbers).

Table 5
Extended Hückel parameters

Atom	Orbital	H_{ii} (eV)	ζ_{i1}	c_1	ζ_{i2}	c_2
Zr	5*s*	−8.52	1.82			
	5*p*	−4.92	1.78			
	4*d*	−8.63	3.84	0.6207	1.510	0.5793
Cr	4*s*	−8.66	1.70			
	4*p*	−5.24	1.70			
	3*d*	−11.22	4.95	0.5058	1.800	0.6747
Si	3*s*	−17.30	1.383			
	3*p*	−9.20	1.383			

2.3. Electrical resistivity

Cold-pressed pellets of $M_2Cr_4Si_5$ (M = Ti, Zr, Hf) each with a diameter of 3 mm and a thickness of 0.5 mm were mounted in a van der Pauw configuration for ac resistivity measurements between 2 and 300 K on a Quantum Design PPMS system equipped with an ac-transport controller (Model 7100). A current of 0.1 mA and a frequency of 16 Hz were used. Measurements were repeated twice on each compound and gave reproducible results.

2.4. Magnetic measurements

Ground samples were placed in gelcap sample holders and dc susceptibility measurements were made under zero-field-cooled conditions with an applied field of 5000 Oe on a Quantum Design 9T–PPMS dc magnetometer/ac susceptometer between 2 and 300 K. The susceptibility was corrected for contributions for the holder diamagnetism and the underlying sample diamagnetism.

2.5. Band structure

A tight-binding extended Hückel band structure calculation on $Zr_2Cr_4Si_5$ was performed with use of the EHMACC suite of programs [16,17]. The atomic parameters are listed in Table 5. Properties were extracted from the band structure using 162 k-points in the irreducible portion of the Brillouin zone.

3. Results and discussion

3.1. Structure

Powder X-ray diffraction data reveal that $Ti_2Cr_4Si_5$, $Zr_2Cr_4Si_5$, and $Hf_2Cr_4Si_5$ adopt the $Nb_2Cr_4Si_5$-type structure, an ordered variant of the binary V_6Si_5-type structure. In the isotypic ternary silicides, the transition-

metal atoms can be distributed over three possible sites. The powder diffraction patterns for $Zr_2Cr_4Si_5$ and $Hf_2Cr_4Si_5$ are sharp whereas that for $Ti_2Cr_4Si_5$ shows distinct peak broadening. This is suggestive of some disorder of the metal atoms in $Ti_2Cr_4Si_5$, although the similar scattering factors of Ti and Cr and the absence of suitable specimens for single-crystal X-ray analysis precluded a definitive answer. In the single-crystal structure of $Zr_2Cr_4Si_5$ (Fig. 1), the Zr and Cr1 atoms lie at the vertices of Si3-centered square antiprisms, whereas the Cr2 atoms lie at the center of octahedra formed by Si1 and Si2 atoms. The square antiprisms share opposite faces and extend along the *c* direction to form one-dimensional chains $^1_\infty[Zr_{4/2}Cr_{4/2}Si]$. The octahedra share faces along the *c* direction and edges along the *a* direction to form layers $^2_\infty[CrSi_{4/4}Si_{2/2}]$. Typical of intermetallic structures, the coordination numbers of the metal atoms are high (CN17 for Zr; CN15 for Cr1; CN14 for Cr2) and consistent with expectations, the larger Zr atom occupies the site with higher CN. The Zr–Si distances (2.642(3)–2.819(1) Å) are generally longer than the Cr–Si distances (2.416(3)–2.583(2); 2.830(2) Å); these are comparable to the Zr–Si distances (2.741–2.900 Å) and the Cr–Si distances (2.406–2.523 Å) found in $ZrCrSi_2$ [18]. There are also extensive metal–

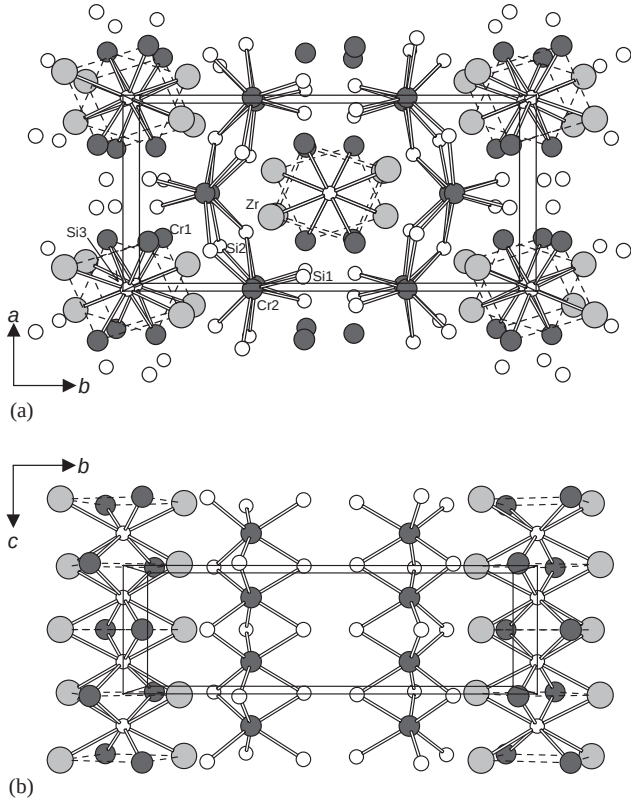

Fig. 1. Views of $Zr_2Cr_4Si_5$ (a) down the *c*-axis and (b) down the *a*-axis. The large lightly shaded circles are Zr atoms, the medium solid circles are Cr atoms, and the small open circles are Si atoms. Some bonds have been omitted for clarity.

metal bonding interactions (Zr–Cr, 2.989(1)–3.418(2) Å; Zr–Zr, 3.111(1) Å; Cr–Cr, 2.5004(4)–3.185(2) Å) whose shortest values correspond well with the sum of the metallic radii (Zr, 1.60 Å; Cr, 1.28 Å) [19]. The $^2_\infty[CrSi_{4/4}Si_{2/2}]$ layers are linked together via rather short 2.354(5) Å and longer 2.742(2) Å Si1–Si1 bonds; within the layers are longer 2.872(3) Å Si2–Si2 distances. The $^1_\infty[Zr_{4/2}Cr_{4/2}Si]$ chains also entail Si3–Si3 distances of 2.5004(4) Å, equal to half of the *c* parameter. These distances are comparable to those found in elemental Si (~2.35 Å) [20] and within Si2 pairs in other silicides (~2.8 Å) [21].

In its conventional description, the V_6Si_5 structure is regarded as a juxtaposition of motifs appearing in the tetragonal V_5Si_3 (W_5Si_3-type) and hexagonal V_5Si_3 (Mn_5Si_3-type) structures [8]. What has escaped attention is the close relationship between this structure and that of Ta_4SiTe_4 [11]. Fig. 2 shows clearly that there is a *klassengleiche* group–subgroup relation, $Ibam \xrightarrow{k2} Pbam$, on going from $Zr_2Cr_4Si_5$ to Ta_4SiTe_4. In both structures, there are Si-centered square antiprisms with metal atoms at the vertices. Additional nonmetal atoms bridge the metal atoms around the square antiprisms, resulting in $^1_\infty[(Ta_4Si)Te_4]$ chains in Ta_4SiTe_4 or in $^1_\infty[(Zr_2Cr_2Si)Si_4]$ chains in $Zr_2Cr_4Si_5$. In Ta_4SiTe_4, these chains interact only weakly through van der Waals forces and are separated by rather open channels. In $Zr_2Cr_4Si_5$, there are two important differences: (i) interstitial octahedral sites between the chains are occupied by additional Cr atoms, and (ii) short Si–Si bonds (not shown in Fig. 2(b)) are formed between the chains. Both of these effects are accompanied by a significant contraction of the cell parameters in $Zr_2Cr_4Si_5$ compared to those in Ta_4SiTe_4, more than can be accounted for by the replacement of Si for Te.

3.2. Properties

Table 6 summarizes electrical resistivity and magnetic susceptibility data for $M_2Cr_4Si_5$ (M = Ti, Zr, Hf). All members show metallic behavior with small resistivity ratios ($\rho_{300}/\rho_2 = 1.2-1.3$) and essentially temperature-independent paramagnetism (the low-temperature Curie tails are attributed to impurities) (Fig. 3). Although there can be large errors associated with the absolute values of the resistivity and susceptibility, it is interesting that the most resistive compound, $Ti_2Cr_4Si_5$, is also the least magnetic.

3.3. Bonding

Both $Zr_2Cr_4Si_5$ and Ta_4SiTe_4 are characterized by extensive metal–metal bonding, but like other V_6Si_5-type structures, $Zr_2Cr_4Si_5$ also contains a range of Si–Si bonding interactions. To a first approximation, the Si1 atom can be assigned an oxidation number of −3, if the

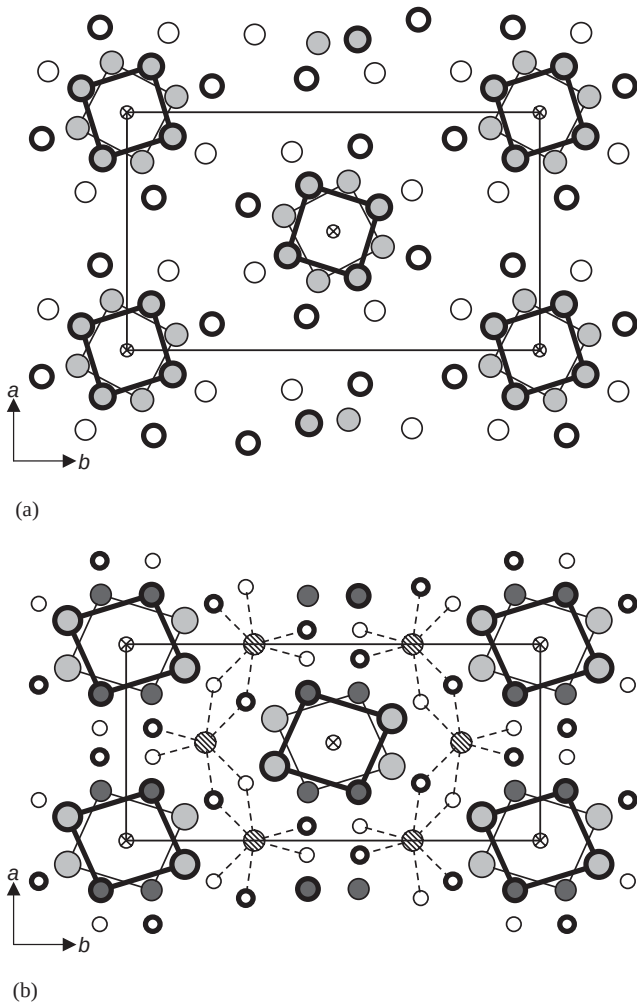

Fig. 2. Comparison of the structures of (a) Ta_4SiTe_4 (*Pbam*) and (b) $Zr_2Cr_4Si_5$ (*Ibam*) in terms of one-dimensional chains of face-sharing Si-centered square antiprisms, shown in projection down the *c*-axis. Light and heavy lines indicate a displacement by 1/2 the repeat along the projection axis. In (a), the large shaded circles are Ta atoms, the small crossed circles are Si atoms, and the medium open circles are Te atoms; in (b), the large shaded circles are Zr atoms, the medium solid or hatched circles are Cr atoms, and the small open or crossed circles are Si atoms.

Table 6
Electrical and magnetic data for $M_2Cr_4Si_5$ (M = Ti, Zr, Hf)

Compound	ρ_{300} (Ω cm)	ρ_5 (Ω cm)	χ_m (emu/f.u.)
$Ti_2Cr_4Si_5$	1.2×10^{-2}	1.0×10^{-2}	2.9×10^{-3}
$Zr_2Cr_4Si_5$	4.6×10^{-3}	3.6×10^{-3}	4.4×10^{-3}
$Hf_2Cr_4Si_5$	8.6×10^{-3}	6.6×10^{-3}	3.8×10^{-3}

short 2.354(5) Å distance within the Si1–Si1 pair is considered to be a 2c–2e$^-$ bond, and all other Si atoms are assigned an oxidation number of −4. In the resulting formulation $(Zr^{3+})_2(Cr^{3+})_4(Si^{3-})_2(Si^{4-})_3$, electron transfer occurs from the metal to the nonmetal atoms, but there are still valence electrons available on the

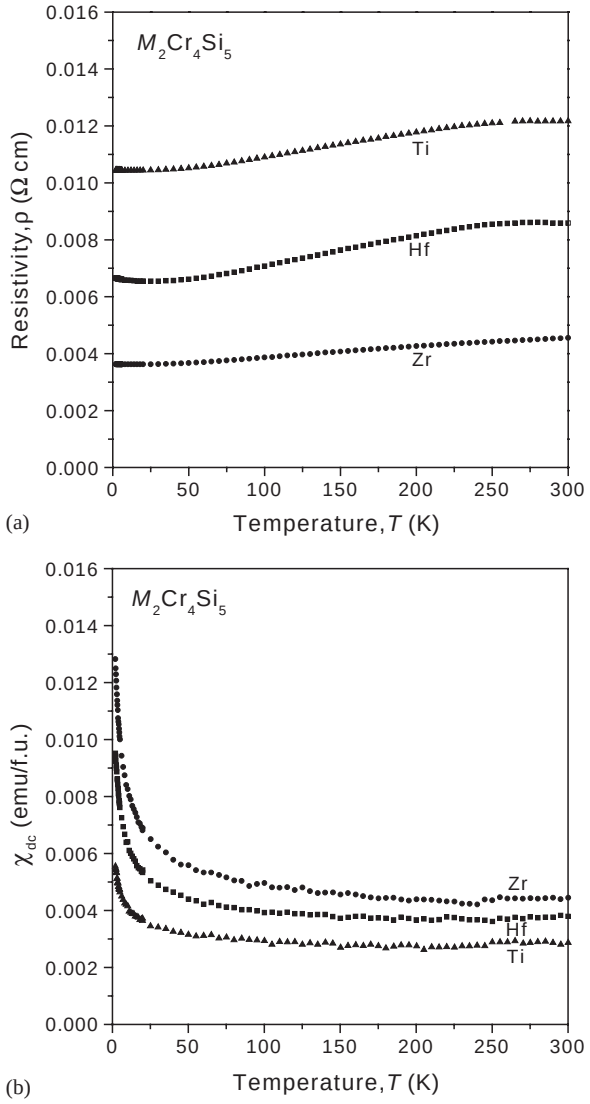

Fig. 3. Plots of (a) electrical resistivity on pressed pellets and (b) dc magnetic susceptibility of powder samples of $M_2Cr_4Si_5$ (M = Ti, Zr, Hf).

metal atoms to form Zr–Zr, Zr–Cr, and Cr–Cr bonds. When Si in $Zr_2Cr_4Si_5$ is substituted by Te in Ta_4SiTe_4, the corresponding formulation $(Ta^{3+})_4(Si^{4-})(Te^{2-})_4$ implies that there is no need to form Te–Te bonds to satisfy the octets of the nonmetal atoms.

The band structure of $Zr_2Cr_4Si_5$ was calculated and the density of states (DOS) curve is shown in Fig. 4. In agreement with the observed metallic behavior of $Zr_2Cr_4Si_5$, there is no band gap at the Fermi level ($\varepsilon_f = -10.27$ eV). The bands responsible for conduction are composed largely of contributions from Cr levels, with minor contributions from Zr levels and virtually none from Si levels. The general features of the DOS curve are consistent with expectations. There are partially occupied Zr 4d and Cr 3d states below the Fermi level that are available for metal–metal bonding. The narrow peak near −10 eV in the DOS curve

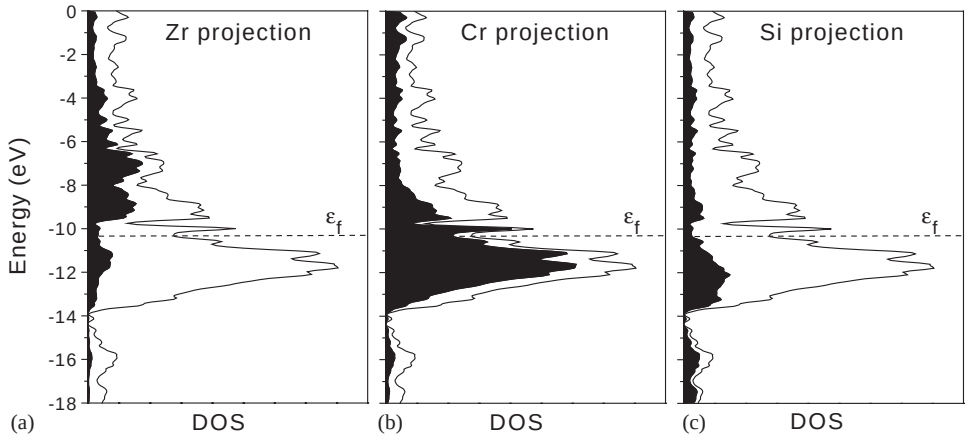

Fig. 4. DOS curve for $Zr_2Cr_4Si_5$ and its (a) Zr, (b) Cr, and (c) Si projections (shaded regions).

originates largely from unfilled e_g levels of the octahedrally coordinated Cr2 atoms. The inserted Cr2 atoms are able to participate in orbital overlap with the surrounding Si1 and Si2 atoms of the hypothetical host structure "$Zr_2Cr_2Si_5$".

Significant mixing of states takes place from −14 to −8 eV, corresponding to strong covalent character of the bonds between Zr, Cr, and Si atoms. This is confirmed by inspection of the crystal orbital overlap population (COOP) curves shown in Fig. 5. Interestingly, the structure achieves stability by optimizing Cr–Si, Zr–Cr, and Cr–Cr bonds (with Mulliken overlap populations (MOP) of 0.28, 0.10, and 0.31, respectively), since their bonding levels are just filled, at the expense of Zr–Si, Zr–Zr, and Si–Si bonds (MOP 0.21, 0.10, and 0.31, respectively), where some bonding levels remain unfilled.

The Zr–Cr bonds can be regarded as donor–acceptor interactions, engendering an electron transfer from Zr to Cr atoms that was not evident in the Zintl formulation provided earlier. In the $^1_\infty[Zr_{4/2}Cr_{4/2}Si]$ chains of square antiprisms (Fig. 1), the Zr and Cr1 atoms are ordered in such a way that the Zr atoms face the Cr2 atoms within the adjacent $^2_\infty[CrSi_{4/4}Si_{2/2}]$ layers to maximize Zr–Cr interactions. When the band structure calculation was carried out with the alternative ordering, where the positions of the Zr and Cr1 atoms are reversed, the structure is destabilized by 7.2 eV.

The homonuclear Cr–Cr and Si–Si interactions are important in $Zr_2Cr_4Si_5$. The one-dimensionality so characteristic of Ta_4SiTe_4 [10] is lost because strong 2.354(5) Å Si1–Si1 (MOP 0.51) and weaker 2.872(3) Å Si2–Si2 bonds (MOP 0.24) develop between the chains of square antiprisms and octahedra. However, there are still significant 2.5004(4) Å Cr–Cr (MOP 0.31) and Si–Si bonds (MOP 0.45) within these chains.

In conclusion, the structure of $Zr_2Cr_4Si_5$ involves Cr atoms occupying octahedral interstices within a hypothetical host structure "$(Zr_2Cr_2)SiSi_4$" similar to

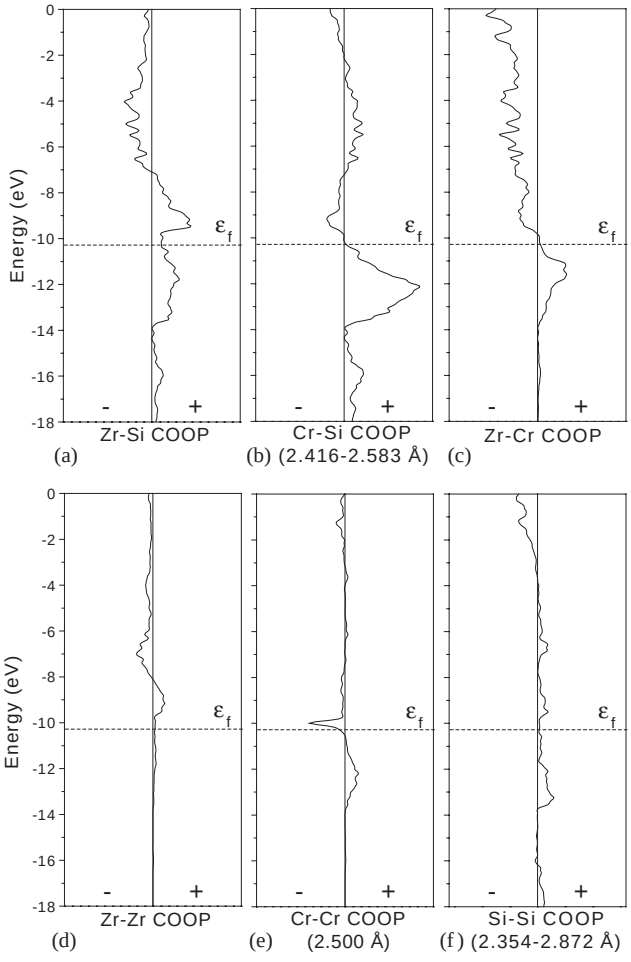

Fig. 5. COOP curves for various bonding interactions in $Zr_2Cr_4Si_5$.

Ta_4SiTe_4 but with the formation of additional Si–Si bonds. Given that the Si atoms in Ta_4SiTe_4 can be replaced by other elements such as Fe, Co, and Ni [11], it may be feasible to attempt the preparation of an analogous derivative with another interstitial element

within the square antiprisms in $Zr_2Cr_4Si_5$, such as "$Zr_2Cr_4FeSi_4$".

Acknowledgments

The Natural Sciences and Engineering Research Council of Canada and the University of Alberta supported this work. We thank Dr. Robert McDonald (Faculty Service Officer, X-ray Crystallography Laboratory) for the X-ray data collection and Ms. Christina Barker (Department of Chemical and Materials Engineering) for assistance with the EDX analyses.

References

[1] P.I. Kripyakevich, Ya.P. Yarmolyuk, E.I. Gladyshevskii, Sov. Phys. Crystallogr. (Engl. Transl.) 13 (1969) 677.
[2] J. Hallais, Ann. Chim. (Paris) 6 (1971) 321.
[3] L.A. Lysenko, V.Ya. Markiv, O.V. Tsybukh, E.I. Gladyshevskii, Izv. Akad. Nauk SSSR, Neorg. Mater. 7 (1971) 175.
[4] L.A. Lysenko, Ya.P. Yarmolyuk, M.M. Paranchuk, Visn. L'viv. Derzh. Univ., Ser. Khim. 17 (1975) 33.
[5] J. Steinmetz, B. Roques, J. Less-Common Met. 52 (1977) 247.
[6] B.Ya. Kotur, M. Sikirica, J. Less-Common Met. 83 (1982) L29.
[7] B.Ya. Kotur, Inorg. Mater. (Engl. Transl.) 23 (1987) 493.
[8] P. Spinat, R. Fruchart, P. Herpin, Bull. Soc. Fr. Minér. Cristallogr. 93 (1970) 23.
[9] M. Wang, W.C. Sheets, R. McDonald, A. Mar, Inorg. Chem. 40 (2001) 5199.
[10] J. Li, R. Hoffmann, M.E. Badding, F.J. DiSalvo, Inorg. Chem. 29 (1990) 3943.
[11] M.E. Badding, F.J. DiSalvo, Inorg. Chem. 29 (1990) 3952.
[12] N. Soheilnia, A. Assoud, H. Kleinke, Inorg. Chem. 42 (2003) 7319.
[13] POLSQ: Program for least-squares unit cell refinement, modified by D. Cahen and D. Keszler, Northwestern University, 1983.
[14] G.M. Sheldrick, SHELXTL Version 5.10, Bruker AXS Inc., Madison, WI, 1998.
[15] L.M. Gelato, E. Parthé, J. Appl. Crystallogr. 20 (1987) 139.
[16] M.-H. Whangbo, R. Hoffmann, J. Am. Chem. Soc. 100 (1978) 6093.
[17] R. Hoffmann, Solids and Surfaces: A Chemist's View of Bonding in Extended Structures, VCH Publishers, New York, 1988.
[18] Ya.P. Yarmolyuk, M. Sikirica, L.G. Aksel'rud, L.A. Lysenko, E.I. Gladyshevskii, Kristallografiya 27 (1982) 1090.
[19] L. Pauling, The Nature of the Chemical Bond, 3rd Edition, Cornell University Press, Ithaca, NY, 1960.
[20] J. Donohue, The Structures of the Elements, Wiley, New York, 1974.
[21] M. Wang, A. Mar, Chem. Mater. 11 (1999) 3232.